BJ Structure

Biochem. J. (2013) **450**, 275–283 (Printed in Great Britain) doi:10.1042/BJ20121773

online data

SUPPLEMENTARY ONLINE DATA

Exploring the sequence–structure relationship for amyloid peptides

Kyle L. MORRIS*, Alison RODGER†, Matthew R. HICKS‡, Maya DEBULPAEP§, Joost SCHYMKOWITZ‖, Frederic ROUSSEAU‖ and Louise C. SERPELL*

*School of Life Sciences, University of Sussex, Falmer, East Sussex BN1 9QG, U.K., †Department of Chemistry, University of Warwick, Coventry CV4 7AL, U.K., ‡School of Biosciences, University of Birmingham, Birmingham B15 2TT, U.K., §VIB Switch Laboratory, Free University of Brussels, Pleinlaan 2, Brussels 1050, Belgium, and ‖VIB Switch Laboratory, Department of Cellular and Molecular Medicine, University of Leuven, Leuven 3000, Belgium

HYFNIF

On the basis of the dimensions of a β-strand monomer of HYFNIF, the available packing arrangements within the determined unit cell (Table S4) are limited and not described by the steric zipper classes. The indexed unit cell may only contain two peptides end on end to satisfy the β-sheet spacing (on the basis of equatorial signal measurement) and appropriately accommodate the length of the peptide. A low-resolution reflection at ~40 Å (Table S3) indicates a longer-range repeat, that we hypothesize arises from a protofilament width. The repeating cell of HYFNIF is well described as two β-strands end on end. Model building explored the possibility of the two β-sheets being related by a displacement along the fibre axis, a rotational symmetry or translation symmetry.

RVFNIM

Two monomers of RVFNIM may be accommodated within the determined unit cell (Table S4). The *a* dimension corresponds approximately to the peptide length and the *b* dimension approximately to double the sheet spacing distance of 10.8 Å. In this respect, this systems arrangement was sufficiently explored by the use of the amyloidogenic class models [6].

VIYKI

Four monomers of VIYKI may be arranged within the repeating cell (Table S4). The *a* dimension corresponds to approximately two peptide β-stands of VIYKI and when considering the β-sheet spacing of 9.21 Å, the *b* dimension can accommodate approximately two β-sheets. This creates a large cell that contains four VIYKI monomers. We consider that this is akin to two amyloid class models side by side and so modelling was based on searching the structure space based on a cell containing two β-strands. The *a* dimension may again correspond to a protofilament width and arise from lateral packing of protofilaments.

[1] To whom correspondence should be addressed (email l.c.serpell@sussex.ac.uk).

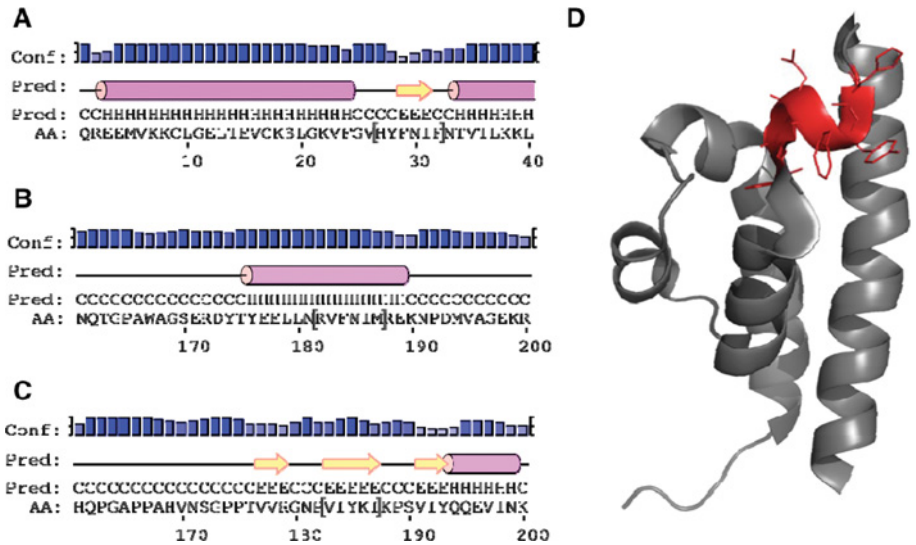

Figure S1 The native sequence context and secondary structures predicted for the Waltz peptides

(**A**) HYFNIF, (**B**) RVFNIM and (**C**) VIYKI in their native full-length sequences. (**D**) The three-dimensional structure of HYFNIF (highlighted in red) in its native structure is shown from PDB code 2KV2 [3]. Secondary structure predictions were made using the online server PSIPred [4,5]. See Table 1 of the main text.

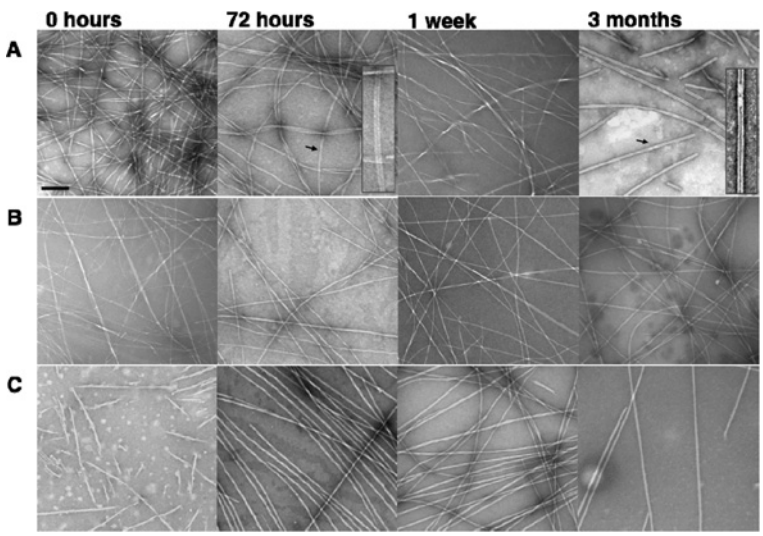

Figure S2 Transmission electron micrographs of the Waltz peptides over time

(**A**) HYFNIF, (**B**) RVFNIM and (**C**) VIYKI are shown at 0 and 72 h to 1 week and 3 months after dissolution. Scale bar, 200 nm. See Figure 1 of the main text.

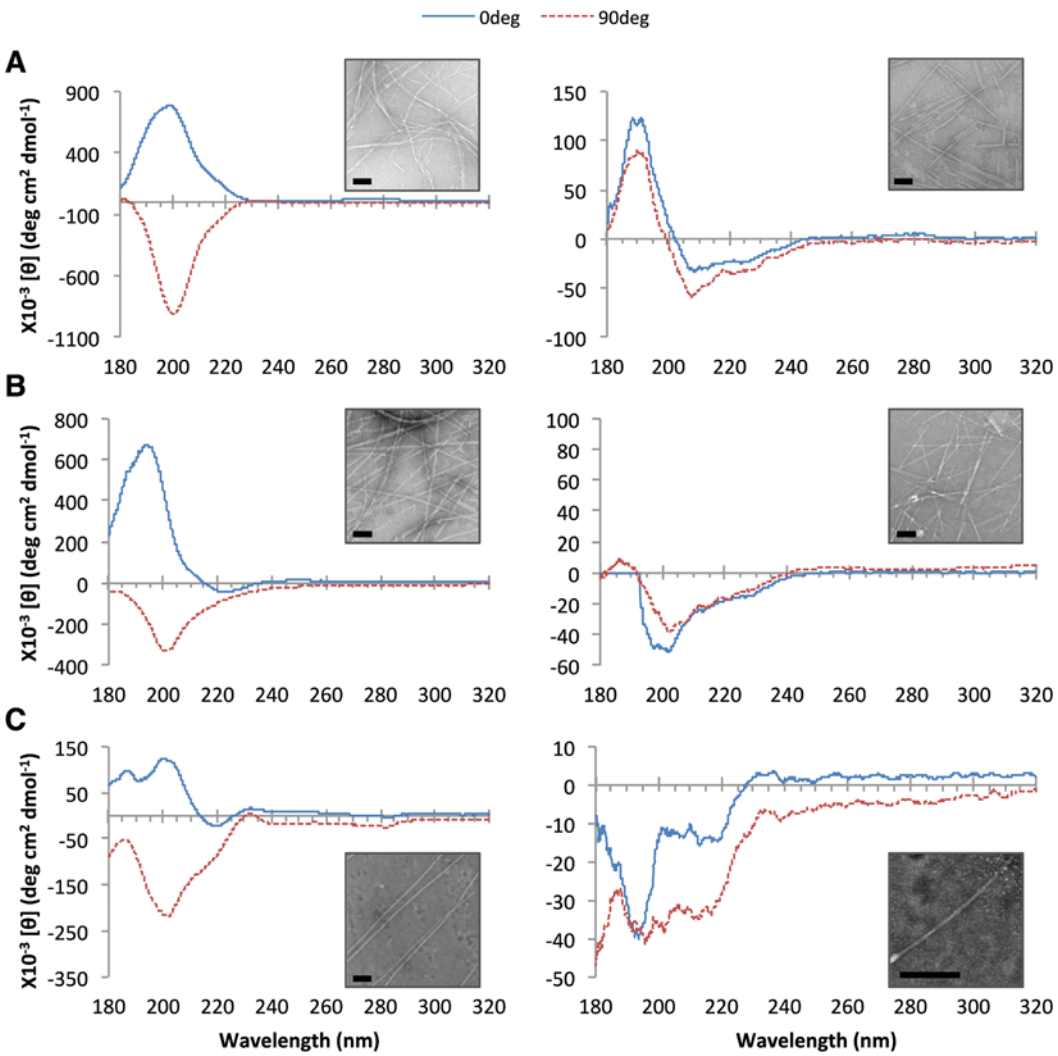

Figure S3 CD spectra for the Waltz peptides pre- and post-sonication

(**A**) HYFNIF, (**B**) RVFNIM and (**C**) VIYKI pre- (left-hand panel) and post- (right-hand panel) bath sonication. The legend indicates sample orientation in the instrument. TEM of the samples are shown as insets; scale bars, 100 nm. LD artefacts are observed in the samples pre-sonication as indicated by sample orientation signal dependence. The true CD signals reveal β-sheet secondary structure with additional contributions from phenylalanine and tyrosine at ~210 nm and ~230 nm respectively, due to the high aromatic content of the Waltz peptides (17–33 %). See Table S1 and Figure 2 of the main text.

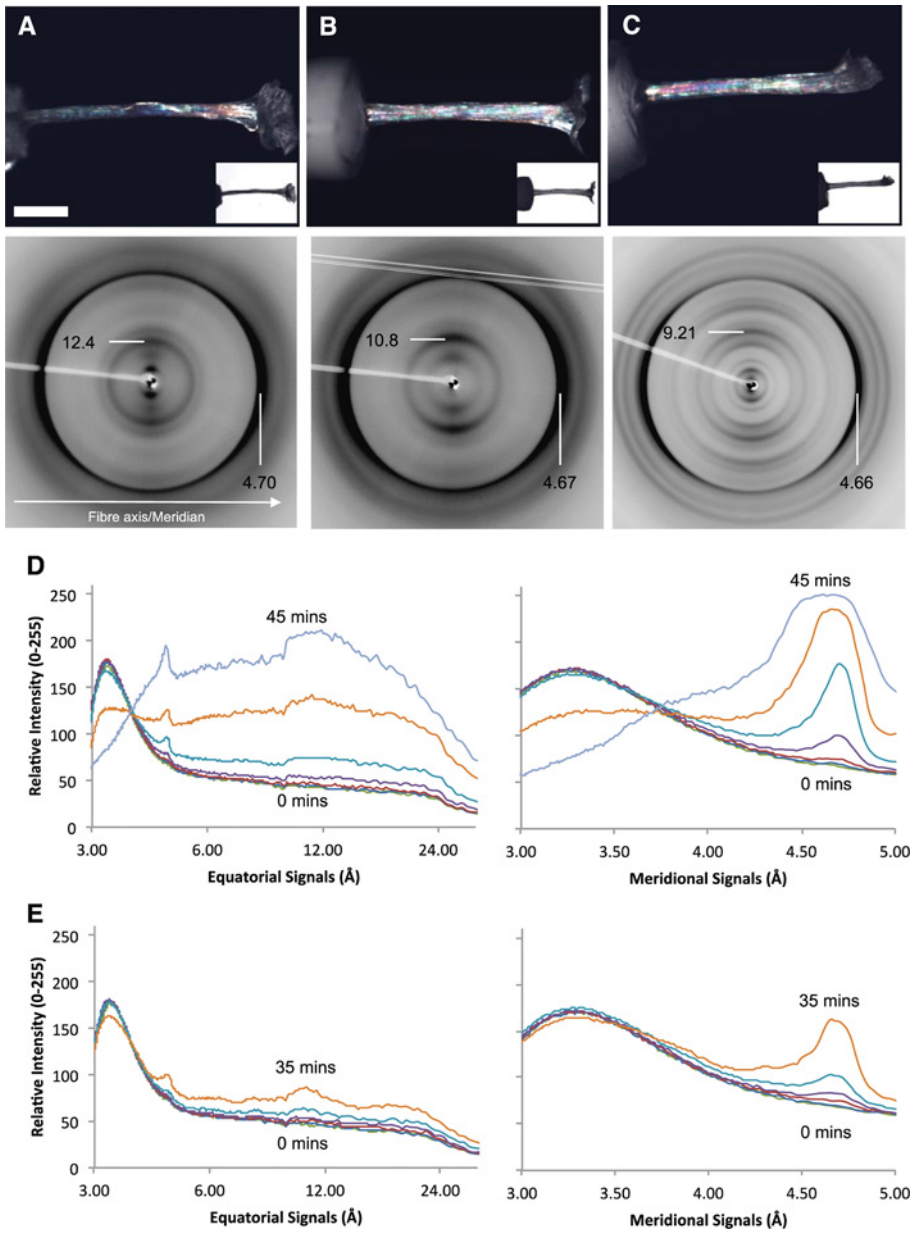

Figure S4 Typical alignments, fibrous and real-time XRFD of the Waltz peptides

(**A**) HYFNIF, (**B**) RVFNIM and (**C**) VIYKI as visualized by cross-polarized microscopy. The insets show the alignments under normal light microscopy. Scale bar, 500 μm. XRFD from the corresponding alignments is shown with major meridional (vertical lines) and equatorial (horizontal lines) reflections labelled in Å. Data were collected at Diamond I24. Real-time XRFD from (**D**) HYFNIF and (**E**) RVFNIM is shown graphically. In both cases the equatorial and meridional signals characteristic of the amyloid structure are observed, amd the diffuse diffraction signal at $\sim$3 Å indicates the alignment is still hydrated. Equatorial signals are shown over a logarithmic scale for clarity. See Figure 4 in the main text.

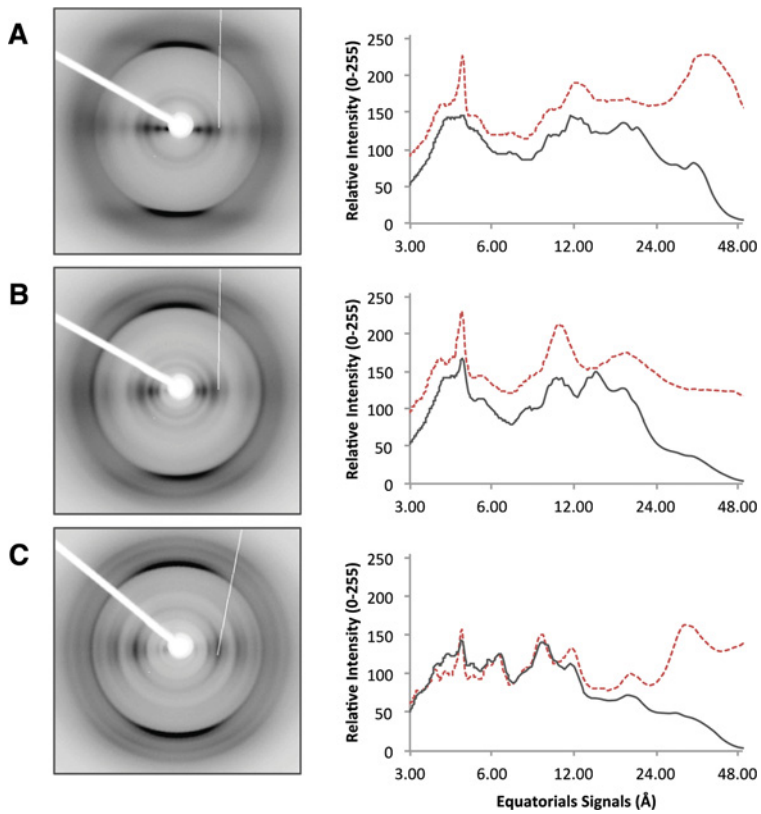

Figure S5 XRFD exhibited from different textured alignments of the Waltz peptides

(**A**) HYFNIF, (**B**) RVFNIM and (**C**) VIYKI in a film-texture. Graphical traces of the equators are shown for comparison of (black line) film-textured to (red dotted line) fibrous-textured alignments. These indicate the same structure is reported with some additional information in the case of RVFNIM, which is later used for comparison with simulation data. Patterns are aligned with equivalent fibre axes vertical and equatorial signals are shown over a logarithmic scale for clarity. See Figure 6 of the main text.

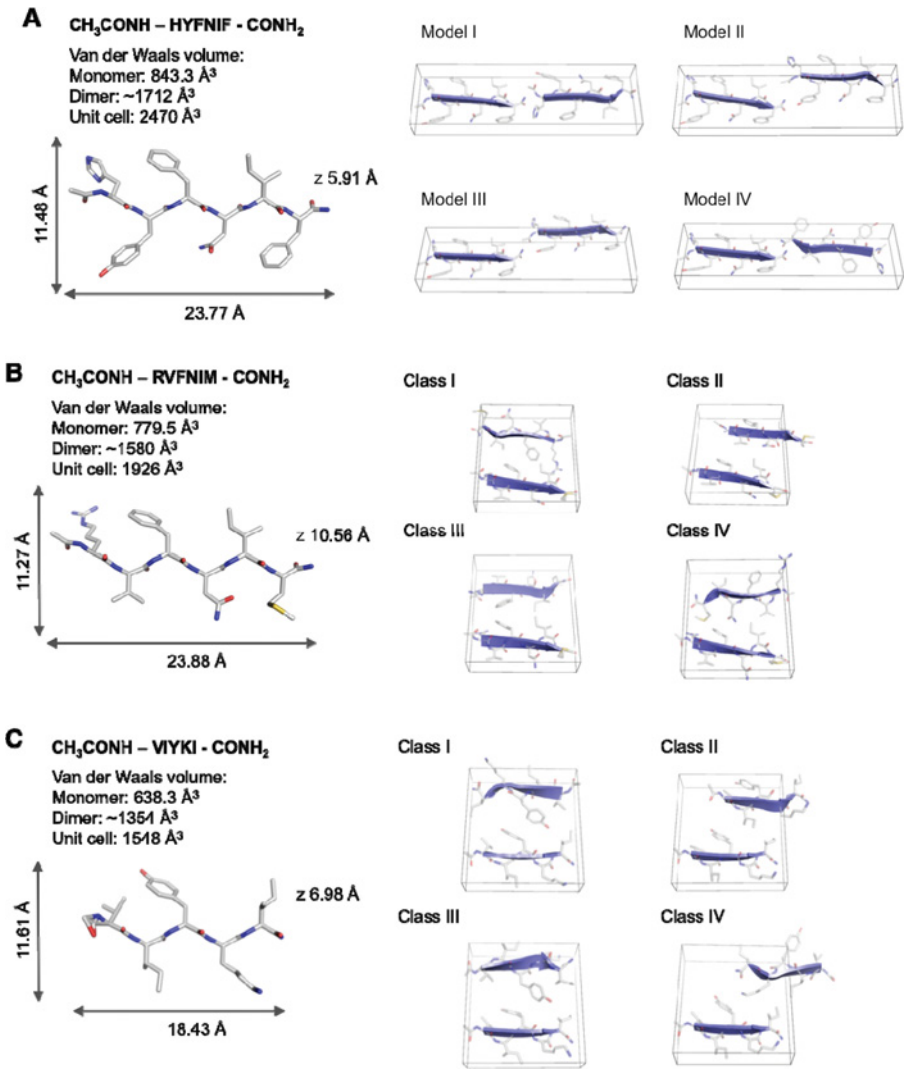

Figure S6 Four structural classes constructed for the three Waltz peptides

(**A**) HYFNIF, (**B**) RVFNIM and (**C**) VIYKI. See Figure 5 of the main text.

Table S1 Dichroweb analysis of the CD spectra recorded for the Waltz peptides post-sonication, highlighting the predominant secondary structural elements

Analysis was performed over two data sets using the CDSSTR analysis program [1] and SP175 190–240 nm reference set [2]. NRMSD, normalized root-mean-square deviation.

	HYFNIF		RVFNIM		VIYKI	
Secondary structure	%	±	%	±	%	±
Helix	6.0	1.4	4.5	2.1	2.0	0.0
Strand	42.5	3.5	40.0	5.7	42.5	0.7
Turn	11.5	0.7	12.5	2.1	12.0	0.0
Other	40.0	1.4	42.5	0.7	41.5	0.7
Total	100.0	7.1	99.5	10.6	98.0	1.4
NRMSD	0.03	0.01	0.05	0.00	0.04	0.01

Table S2 LD peaks exhibited by the Waltz fibrils when under shear and Couette flow alignment

LD and LD_{red} values are reported in $\Delta Abs \times 10^4$ after background subtraction and zeroing. Abs_{iso} are reported as the isotropic absorbance from the sample after background Abs_{iso} subtraction. Shear aligned fibrils are perpendicular to the orientation axis (⊥), whereas flow aligned fibrils are parallel with the orientation axis (//).

	HYFNIF				RVFNIM				VIYKI			
	nm	LD	Abs_{iso}	LD_{red}	nm	LD	Abs_{iso}	LD_{red}	nm	LD	Abs_{iso}	LD_{red}
Shear aligned	283.4	− 3.862	0.003	− 1492	–	–	–	–	283.0	− 8.174	0.017	− 492.3
	278.0	− 4.278	0.004	− 1033	–	–	–	–	276.0	− 7.777	0.020	− 382.2
	234.0	1.881	0.027	69.63	–	–	–	–	231.2	12.16	0.083	146.5
	200.0	− 198.4	0.490	− 404.8	196.4	− 268.7	0.429	− 626.7	200.4	− 200.1	0.628	− 318.7
Flow aligned	282.6	18.68	0.004	4861	–	–	–	–	283.0	4.655	0.011	429.1
	277.2	19.61	0.005	3794	–	–	–	–	276.0	3.878	0.014	272.0
	234.4	− 10.53	0.026	− 399.6	–	–	–	–	231.6	− 8.625	0.064	− 135.1
	200.4	964.4	0.491	1963	–	–	–	–	200.0	98.65	0.525	187.9

Table S3 XRFD signals exhibited from fibrous alignments of HYFNIF, RVFNIM and VIYKI

Reflections measured manually are indicated by *. E, equatorial; M, meridional; Rad, radially averaged.

HYFNIF			RVFNIM			VIYKI		
Signal (Å)	Normalized relative intensity	Axis	Signal (Å)	Normalized relative intensity	Axis	Signal (Å)	Normalized relative intensity	Axis
38.98	0.95	E				33.26*	0.47	E
19.22	0.70	E	18.72	0.73	E	20.04	0.29	E
12.37	0.78	E	10.79	0.87	E	11.81	0.38	E
10.03	0.63	E	8.31*	0.62	E	9.21	0.43	E
7.05	0.50	E	5.48	0.59	E	8.09*	0.34	E
5.23	0.60	E				6.35	0.36	E
						5.82*	0.34	E
						5.12	0.28	E
						3.25*	0.22	E
4.70	1.00	M	4.67	1.00	M	4.66	1.00	M
3.95	0.66	Rad	2.38	0.27	M	4.01	0.34	M
2.38	0.20	M				3.72	0.34	Rad
						2.38*	0.10	M

Table S4 The diffraction signals and their respective indexing to the modelled unit cells predicted by Clearer

[0 0 1] indices correspond to the fibre axis, all others are perpendicular to the fibre axis. The unit cell dimensions correspond to the peptides as follows: $a = \beta$-strand long axis, $b = \beta$-sheet spacing and $c = \beta$-sheet hydrogen bonding distance/fibre axis. The intensity of the 011 reflection is increased for RVFNIM and VIYKI due to β-sheet displacement along the fibre axis leading to higher resolution observed major meridional values.

HYFNIF					RVFNIM					VIYKI				
	a (Å) 41.72	*b* (Å) 12.60	*c* (Å) 4.70	$\alpha = \beta = \gamma$ 90°		*a* (Å) 18.80	*b* (Å) 21.94	*c* (Å) 4.78	$\alpha = \beta = \gamma$ 90°		*a* (Å) 34.94	*b* (Å) 19.01	*c* (Å) 4.76	$\alpha = \beta = \gamma$ 90°
Indexing														
Obs	h	k	l	Calc	Obs	h	k	l	Calc	Obs	h	k	l	Calc
38.98	1	0	0	41.72	18.72	1	0	0	18.80	33.26	1	0	0	34.95
19.22	2	0	0	20.86	10.79	0	2	0	10.97	20.04	0	1	0	19.01
12.37	0	1	0	12.60	8.31	2	1	0	8.64	11.81	3	0	0	11.65
10.03	4	0	0	10.43	5.48	0	4	0	5.49	9.21	1	2	0	9.17
7.05	6	0	0	6.95	4.67	0	0	1	4.78	8.09	4	1	0	7.94
5.23	8	0	0	5.22	4.67	0	1	1	4.67	6.35	0	3	0	6.34
4.70	0	0	1	4.70	2.38	0	0	2	2.39	5.82	6	0	0	5.82
4.70	1	0	1	4.67						5.12	4	3	0	5.13
3.95	6	0	1	3.89						3.25	8	4	0	3.22
2.38	0	0	2	2.35						4.66	0	0	1	4.76
										4.66	0	1	1	4.62
										4.01	2	2	1	4.14
										2.38	0	0	2	2.38

Table S5 Quantitative RF comparisons of the simulated with the experimental fibre diffraction data

HYFNIF	RF	RVFNIM	RF	VIYKI	RF
Model I	0.37	Class I	0.33	Class I	0.41
Model II	0.38	Class II	0.35	Class II	0.33
Model III	0.34	Class III	0.39	Class III	0.50
Model IV	0.35	Class IV	0.32	Class IV	0.47

REFERENCES

1 Compton, L. A. and Johnson, W. C. (1986) Analysis of protein circular-dichroism spectra for secondary structure using a simple matrix multiplication. Anal. Biochem. **155**, 155–167

2 Lees, J. G., Miles, A. J., Wien, F. and Wallace, B. A. (2006) A reference database for circular dichroism spectroscopy covering fold and secondary structure space. Bioinformatics **22**, 1955–1962

3 Kim, Y. M. and Choi, B.-S. (2010) Structure and function of the regulatory HRDC domain from human Bloom syndrome protein. Nucleic Acids Res. **38**, 7764–7777

4 Jones, D. T. (1999) Protein secondary structure prediction based on position-specific scoring matrices. J. Mol. Biol. **292**, 195–202

5 Buchan, D. W. A., Ward, S. M., Lobley, A. E., Nugent, T. C. O., Bryson, K. and Jones, D. T. (2010) Protein annotation and modelling servers at University College London. Nucleic Acids Res. **38**, 563–568

6 Sawaya, M. R., Sambashivan, S., Nelson, R., Ivanova, M. I., Sievers, S. A., Apostol, M. I., Thompson, M. J., Balbirnie, M., Wiltzius, J. J., McFarlane, H. T. et al. (2007) Atomic structures of amyloid cross-β spines reveal varied steric zippers. Nature **447**, 453–457

Received 23 November 2012/17 December 2012; accepted 20 December 2012
Published as BJ Immediate Publication 20 December 2012, doi:10.1042/BJ20121773